J Nanostruct 15(2): 639-651, Spring 2025

RESEARCH PAPER

Synthesis of Spinal $CoFe_2O_4$ Nanoparticles Assitael with Cetramide and Applied in Removal of Direct Orange 39 Dye

Mohammed F. Hateef [1,2], ***Hasan F. Alesary*** [2], ***Luma M. Ahmed*** [2,3*], ***Stephen Barton*** [4]

[1] *Oil Department, College of Engineering, University of Kerbala, Karbala, Iraq*

[2] *Department of Chemistry, College of Science, University of Kerbala, Karbala, Iraq*

[3] *Al-Zahraa Center for Medical and Pharmaceutical Research Sciences (ZCMRS), Al-Zahraa University for Women, Karbala, Iraq*

[4] *School of Life Sciences, Pharmacy and Chemistry, Kingston University London, Kingston-upon-Thames, Surrey, UK*

ARTICLE INFO

Article History:
Received 17 January 2025
Accepted 25 March 2025
Published 01 April 2025

Keywords:
Azo direct orang 39 dye
Cetramide
$CoFe_2O_4$
Removal
Spinal

ABSTRACT

A cobalt ferrite nanocomposite is used as an affordable nano-adsorbent in this investigation. It can be deposited easily. This study uses simple adsorption to remove toxic direct orange 39 dye from aqueous solution. This process has been studied using Fourier transform infrared spectroscopy, X-ray diffraction, scanning electron microscopy, and X-ray magnetometer energy-dispersive analysis. The EDX spectra show prominent peaks for iron, suggesting it is somewhat abundant in the composition. This study examined the effectiveness of the adsorbent in removing dye from an aqueous solution based on time, concentration, dosage, temperature, and pH. Analysis showed 44.2% iron, 31.3% oxygen, and 16.6% cobalt, confirming their excellent purity as $CoFe_2O_4$ nanoparticles. Cobalt's atomic ratio to iron was 0.4362, which matches the expected 0.5 stoichiometry. Notably, XRD patterns showed no extra peaks, indicating no contamination. Sample purity was ensured by measuring Bragg reflections between 7.0054 and 79.9904. The sample's cobalt ferrite NPs had cubic unit cell-like peaks, indicating an inverted spinel structure. Using statistical analysis and the Debye-Scherer equation, the crystallite size in $CoFe_2O_4$ was determined to be 30.9 nm. Adsorption efficacy was strongly correlated with temperature, with the maximum efficiency of 97.82% at 10°C. The perfect removal of 5 ppm of direct orange 39 dye using 0.025 g of $CoFe_2O_4$ NPs turned into pH 6 at 45 min. The ΔH^o of adsorption is -87.6462 kJ/mol (exothermic) which emphasizes energy release, moderate interaction strength, and favorable adsorption; efficiency reduces with higher temperatures. The $CoFe_2O_4$ adsorbent can be reused for a maximum of three cycles.

How to cite this article
Hateef M., Alesary H., Ahmed L., Barton S. Synthesis of Spinal $CoFe_2O_4$ Nanoparticles Assitael with Cetramide and Applied in Removal of Direct Orange 39 Dye. J Nanostruct, 2025; 15(2):639-651. DOI:10.22052/JNS.2025.02.024

INTRODUCTION

The advantageous magnetic, optical, and antibacterial properties of magnetic nanoparticles have recently begun to garner significant attention in most biological fields related to human life. They demonstrated their efficacy against bacterial pathogens, highlighting eco-friendly and biocompatible properties with potential in health care and environmental fields [1]. The integration of artificial intelligence (AI) into nanotechnology has revolutionized research and development, enabled precise predictions of nanoparticle

---

[*] *Corresponding Author Email: luma.ahmed@uokerbala.edu.iq*

properties, optimized synthesis conditions, and reduced experimental costs and time. This synergy between AI and nanotechnology has opened new avenues for applications in environmental remediation, biomedicine, and advanced material development [2]. One of the strongest magnetic materials, ferrite, is made up of two types of spinel structure: inverse and normal. Cobalt ferrite's inverse spinel structure offers several benefits, including high magnetostrictivity, low cost, and good coupling efficiency. Among the materials most frequently utilized as colorants in scientific and commercial processes are pigments and dyes. Specifically, they are extensively utilized in the printing and leather sectors, as well as in the spheres of plastics, foodstuffs, papers, cosmetics, and pharmaceutical products [3-6]. The global production of dyes and pigments has increased by over 700,000 metric tons annually (which proves the continuous annual rise rather than a cumulative total over multiple years), with there now being over 10,000 different types; however, 10-15% of these dyes will ultimately be allowed to leak into the environment. Should this occur, the formation of dangerous products: nitrogen oxides, carbon monoxide (CO), and hydrogen chloride, all of which are toxic to humans and animals due to the toxicity of certain dyes, such as the neutral. Due to this, the problem of dye treatment has received considerable theoretical attention from many researchers. Of the approaches examined, one way is to be cooled before being dumped, implying that cooling is the only necessary step [7-9] In fact, several chemical and physical treatment methods such as chemical oxidation and electrochemical treatment are widely used to remove ions and dyes from wastewaters [10], for instance, precipitation [11], liquid chromatography [12], membrane filtration [13] and correlation [14]. Due to its low cost, ease of preparation and design, and potential for multiple recycling and reuse of the adsorbent, the adsorption process has recently garnered particular attention for treating organic pollutants and dyes in waste effluents [15,16]. Spinals with a high surface area are employed in numerous technical fields, namely pharmaceutical, chemical, electronics, computer, separation, and medical fields as target delivery, catalytic agents, high-density record storage, ferrofluids, magnetic separation, and MRI. The spinel ferrite structure is derived from a closed pack of oxygen ions and has a tetrahedral (A) and an octahedral (B) interstice. The general formula of spinel ferrites is $A_2B_2O_4$ when A and B are representing the cations. In contrast, the Inverse spinals have divalent ions in the octahedral positions such as $NiFe_2O_4$ [17] whereas normal spinals only have divalent ions in the tetrahedral sites such as $ZnFe_2O_4$ [18] Most of the interesting phenomena relating to spinel ferrites originate from so-called cation superexchange, involving octahedral (B) and tetrahedral (A) site cations [19,20]. A more inverted spinel structure is observed for $CoFe_2O_4$ because Co^{2+} ions occupy the B sites while Fe^{3+} ions are distributed in nearly equal proportions between the A and B sites [21]. Cobalt ferrite, a member of the ferrite family, is renowned for its exceptional properties as a hard magnetic material. It possesses excellent magnetostrictive qualities, moderate magnetization, and high coercivity. These characteristics make Co ferrite nanoparticles highly desirable for various technical applications, thanks to their outstanding chemical and physical stability [22]. Their uses include memory cores, high-density information storage, high-frequency devices, and the biomedical industry [23]. This study is interested in synthesizing spinal $CoFe_2O_4$ nanoparticles, in conjunction with the use of cetramide as a template, a capping agent. Furthermore, it is our objective to study the attributes of these nanoparticles through various methods – Fourier-transform infrared spectroscopy (FT-IR), X-ray diffraction (XRD), and Scanning Electron Microscopy with Energy Dispersive X-ray (SEM-EDX), In addition, the efficiency of these nanoparticles shall assess in the elimination of colored organic species, such as the direct orange 39 dye adopted by the textile industry. In this evaluation, factors such as the amount of the catalyst and the initial pH of the solution, as well as its temperature, will be considered.

MATERIALS AND METHODS

Materials and Reagents

To conduct this research, we gathered the necessary materials, including direct orange 39 dye sourced from Hila textile factory. Table 1 provides a detailed description of the specific characteristics of this dye. The powders utilized in the study were ferric nitrate ($Fe\ (NO_3)_{3.}6H_2O$) and cobalt nitrate ($Co\ (NO_3)_3{\cdot}6H_2O$), which were purchased from Sigma Chemical Corp., USA. Hydrochloric acid (35%) was obtained from a general drug house. We also acquired absolute ethanol (C_2H_5OH) cetramide (CT) as a template purchased from Sigma-Aldrich Chemie.

Synthesis of Spinel $CoFe_2O_4$ NP

Using a simple and efficient preparation method (due to its straightforward method, minimal energy requirements, and ability to produce uniform, high-purity $CoFe_2O_4$ nanoparticles with almost controlled size and structure.), $CoFe_2O_4$ nanoparticles were produced in the presence of a surfactant. To begin the synthesis, 13.9 g of ferric nitrate ($Fe(NO_3)_3.6H_2O$) was dissolved in 200 mL distilled water while, separately, 4.14 g of the cobalt nitrate ($Co(NO_3)_2.6H_2O$) was dissolved in 200 clean mL water the cobalt nitrate solution was then gradually added to the ferric nitrate solution with vigorous stirring at room temperature. Following this, 1 g of the surfactant cetramide (CT) (to stabilize nanoparticles, preventing clumping and ensuring uniform size and dispersion) was introduced. After stirring for ten minutes, the product was heated and stirred for a further 10 minutes. To achieve a pH between 9.5 and 10, a specific amount of concentrated ammonia solution was slowly added to the solution while heating and stirring were maintained for 1 h. This resulted in the formation of a dark brown solution, which was subsequently filtered and washed with distilled water and ethanol. The precipitate so obtained was then dried in an oven at 100°C for 1 h. Finally, the precipitate was the precipitate was burned at 300°C. As shown in Fig. 1.

Application of the Spinel $CoFe_2O_4$ NP in Removal of direct orange 39 dyes

Using a shaker set at 50 rpm, a mixture was prepared by adding 0.3 g $CoFe_2O_4$ to 25 mL direct orange 39 dye solution in a beaker. The mixture was shaken for a specific duration to account for variations in contact time, dose, concentration, temperature, and pH when the dye was adsorbed upon the external layer of the $CoFe_2O_4$, both the dye and the magnet were attracted to each other. The proportion of dye remaining in the mixture was then measured using a UV-visible spectrophotometer at a wavelength of 416 nm. The adsorption capacity at equilibrium (q_e) in (mg/g) [25,26]

$$q_e = \frac{(C_o - C_e)V}{m} \tag{1}$$

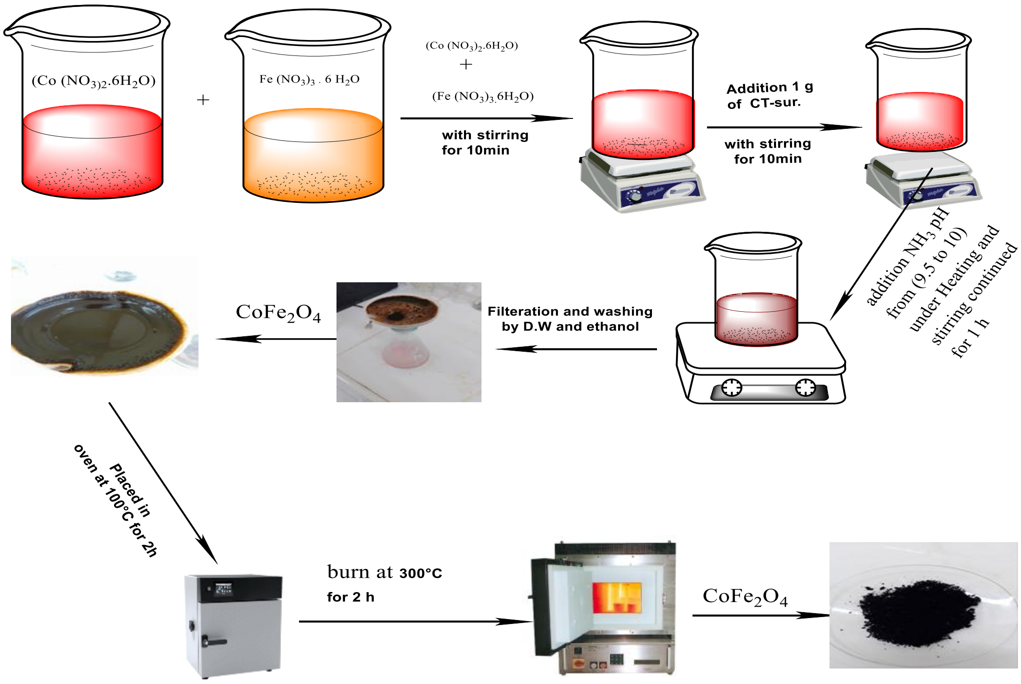

Fig. 1. Schematic diagram of the steps for cobalt ferrite nanoparticle preparation.

The adsorption efficiency E % can be calculated by following the equation:

$$E\,\% = \frac{C_o - C_t}{C_o} \times 100 \qquad (2)$$

Where: C_o is the actual dye concentration in the solution, C_e is the concentration in (mg/L) of dye at time equilibrium is the volume of the dye solution (L), and m is the mass of the adsorbent ($CoFe_2O_4$NPs) used in (g). C_t is the concentration (mg/L) of dye at different times.

RESULTS AND DISCUSSION

Characterization of $CoFe_2O_4$ nanoparticles

To allow for an appropriate examination of the samples synthesized in this research several analyses were conducted, which included FTIR, XRD, FE-SEM, and EDX-elemental analysis.

FT-IR Analysis

FT-IR analysis provided evidence for the development of the spinal form of cobalt ferrite and its distribution of cations. The infrared transmittance spectra of cobalt ferrite samples, obtained at different synthesis temperatures, are shown in Fig. 2. The O-H stretching mode was assigned to the absorption band at 3117.07 cm^{-1} which corresponds to O–H stretching [27,28] The stretching vibration of tetrahedral group complexes is responsible for the presence of various absorption bands [22]. In general, spinals, including ferrites, display distinctive FT-IR spectra characterized by two primary metal-oxygen bands. The spectra indicate the presence of absorption bands in the range of 400 to 600 cm^{-1} which is a common feature of the spinel ferrite [29]. The vibrations associated with the Fe-O tetra site give

Table 1. Some of the features that can be associated with the Direct Orange 39 dye [24].

The variables	Information
Molecular Formula	$C_{12}H_{10}N_3NaO_3S$
Molecular Weight	299.28100 g mol^{-1}
Common Synonyms	Solar Yellow 3R, Orange 2GL
Dye Class	Azo, Direct Dyes
λ_{max}	415 nm

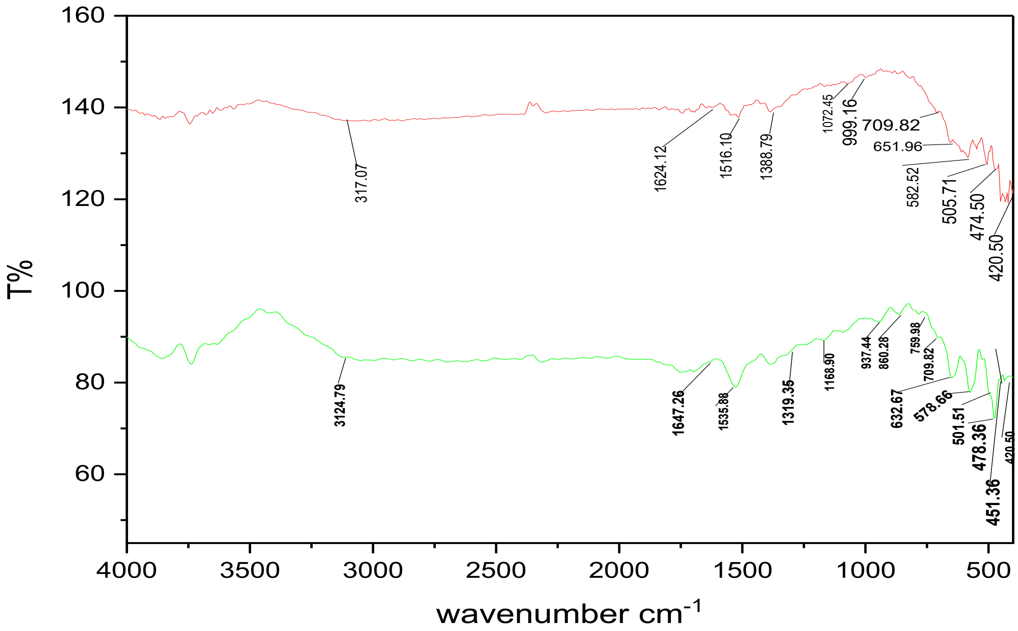

Fig. 2. The FT-IR spectra of $CoFe_2O_4$ NP synthesis.

rise to the highest frequency band, is located at v1 = 709.827-582.52 cm^{-1} corresponds to Fe–O vibrations in tetrahedral and octahedral sites. The absorption band near v2, which is linked to the octahedral 'B' site, is made up of multiple peaks due to the presence of various cations, which include Co (II), Fe (III), and Fe (II), on the 'B' site [30]. The peak in (474.50-420.49) cm^{-1} that corresponds to Co–O bonding, indicates the bonding of cobalt to oxygen. in addition to the peak at 1100 cm^{-1} which is assigned to the O-Fe-O as an octahedron bending [31].

X-ray Diffraction (XRD) Analysis

The X-ray diffraction patterns of $CoFe_2O_4$ have been studied in detail using the X' Pert Pro system. The analysis was carried out under exact parameters, which included an 8-mA current, a 40 kV voltage, and a step size of 0.0110, at a step rate of 1 s per step. No additional peaks were found in the XRD patterns, suggesting the absence of contaminants. Bragg reflections were measured between 7.0054 and 79.9904 to ensure sample purity. The X-ray diffraction profile provided vital information about the synthesized powder sample's qualitative and quantitative phases, in addition to its preferred orientation. Fig. 3 illustrates the X-ray diffraction structure of $CoFe_2O_4$, having peaks at 2θ values of 17.19°, 23°, 29°, 30°, and 45° which correspond to the (111), (220), (311), (222), and (400) reflections of $CoFe_2O_4$, respectively. These findings align with previous research on the synthesis of $CoFe_2O_4$ conducted by other research groups [32-34]. One of the notable properties of the synthesized powders was the absence of any detectable impurity phase, the absence of further peaks indicates particles purity. This suggests that the synthesized $CoFe_2O_4$ nanoparticles consist solely of the desired crystalline phase [31]. The cobalt ferrite NPs in the sample showed peaks that corresponded to the position of a cubic unit cell, indicating an inverse spinel structure (JCPDS No. 98-011-1281). The crystallite size in $CoFe_2O_4$ was determined to be 30.9 nm using statistical analysis and the Debye Scherer equation (Eq. 3) [17,35,36].

$$(\mathrm{L}) = \frac{\mathrm{K}\lambda}{\beta \mathrm{COS}\theta} \tag{3}$$

Where λ = 1.54 Å, k = 0.9 (constant), β = FWHM, θ = 2θ/2, and L represents the average crystallite size (nm).

FE-SEM Analysis

Over many years, scanning electron microscopy (SEM) has remained the favored method for examining the physical attributes and surface characteristics of different materials. This particular technique enables the determination of particle size distribution and shape. In this particular investigation, composite SEM spectra were employed to analyze the surface morphology

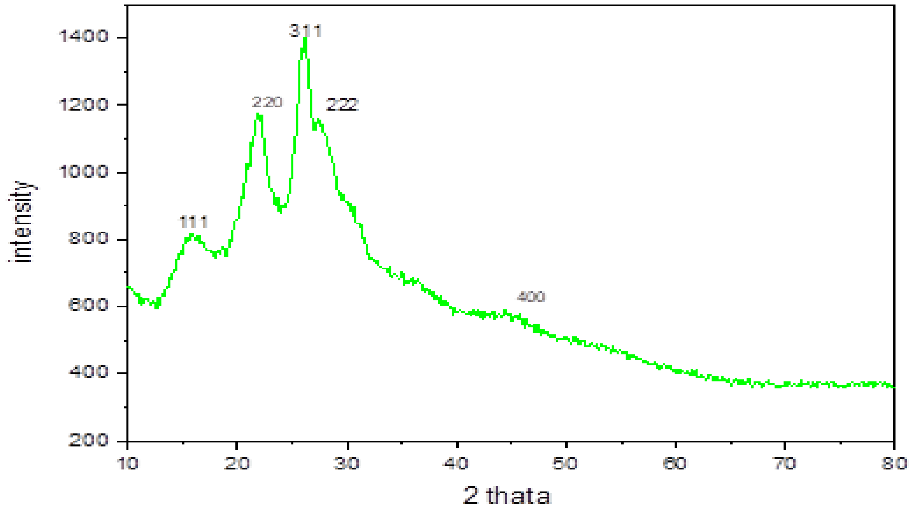

Fig. 3. XRD of $CoFe_2O_4$ NP Synthesis.

of $CoFe_2O_4$ spinel. The introduction of a CT surfactant resulted in a compact arrangement of uniform nanoparticles, forming spherical granules that aggregated into a nanoparticle structure. The average particle size was measured at 41.35 nm, which surpasses the average crystal size due to the prevalence of polycrystalline particles. This can be attributed to the small size and high density of the nanoparticles as illustrated in Fig. 4a. The polycrystalline nature of the $CoFe_2O_4$ structure was verified by conducting energy dispersive X-ray (EDX) analysis to examine the elemental composition. The inclusion of CT surfactants facilitated the synthesis of pure $CoFe_2O_4$ nanoparticles, as illustrated in Fig. 4b. There were no notable variations in particle size, with more particles exhibiting a textured shape. The elemental composition of the synthesized nanoparticles is accurately represented by the peaks observed in the EDX analysis. The results indicate that the nanoparticles are composed solely of cobalt (Co), iron (Fe), and oxygen (O), without any impurities. Notably, the EDX spectra show prominent peaks for iron, suggesting it to be

Table 2 The results of the EDX analysis of $CoFe_2O_4$ nanoparticles are as follows.

Element	Atomic%	Weight %
C	17.8	7.9
O	53.1	31.3
Fe	21.5	44,2
Co	7.7	16.6

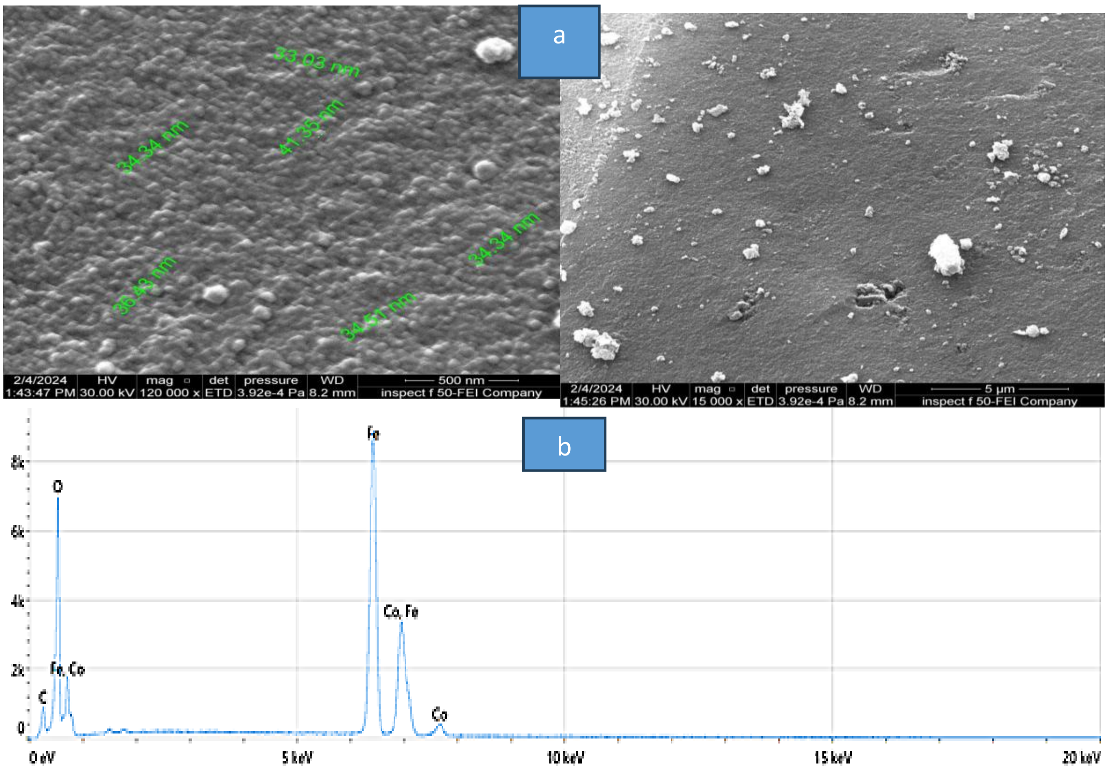

Fig. 4. (a)FE-SEM micrographs of $CoFe_2O_4$ NP. (b) EDX spectrum of $CoFe_2O_4$ NP.

somewhat abundant in the composition Further analysis revealed that the nanoparticles consist of 44.2% iron, 31.3% oxygen, and 16.6% cobalt, as illustrated in Table 2 confirming their high purity as $CoFe_2O_4$ nanoparticles. Additionally, the atomic ratio of cobalt to iron was determined to be 0.4362, which closely aligns with the expected stoichiometry of 0.5 [32,33]. The appearance of an Au peak in the EDX spectral analysis can be ascribed to the procedures of sample preparation and analysis, which entail the application of a layer of Au, enabling conductivity and promoting the movement of electric charge.

Removal of Direct Orange 39 Dye using $CoFe_2O_4$ NPs

Effect of Contact Time

The data in Fig. 5 elucidates the temporal evolution of direct orange 39 dye adsorption by the synthesized $CoFe_2O_4$ nanoparticles. A substantial increase in efficiency of dye removal and adsorption constant values over time signifies the effective adsorption of the dye. Notably, the adsorption efficiency exhibited a significant increase from 27.33% at the initial 15 min to 69.43% after 45 min. concomitantly, the adsorption constant (kd) followed an upward trajectory, peaking at 2.2722 min^{-1} at 45 min. These parameters depress with elevating the contact time that due to desorption the dye from surface [37].

Effect of direct orange 39 concentration on removal process using $CoFe_2O_4$ NP

The removal capacity for direct orange 39 dyes is influenced by the concentration of the dye solution and the amount of $CoFe_2O_4$ catalyst used. 25 mL of dye solution was utilized at concentrations ranging from 5 to 15 ppm. The equilibrium time was set at 30 minutes and the temperature was maintained at lab temperature (25ºC), as shown in Fig. 6. The efficiency of dye removal decreased from 37.1816% to 0.8488% as the initial dye concentration increased from 5 ppm to 15 ppm. This decrease in efficiency can be attributed to the saturation of active sites on the catalyst surface, which occurs when the initial dye concentration increases. Consequently, the adsorption process is slowed considerably [38,24].

Effect of $CoFe_2O_4$ NP Dose on direct orange 39 dye Removal Process

Adsorption was utilized to remove 25 ppm of straight orange-39 dyes, employing $CoFe_2O_4$ as the adsorbent. The dosage of $CoFe_2O_4$ ranged from 0.1 g to 0.4 g per 100 mL for 45 minutes. As depicted in Fig. 7, the dye removal process exhibited an upward trend with increasing mass of $CoFe_2O_4$, ultimately reaching a removal efficiency of 82.34%

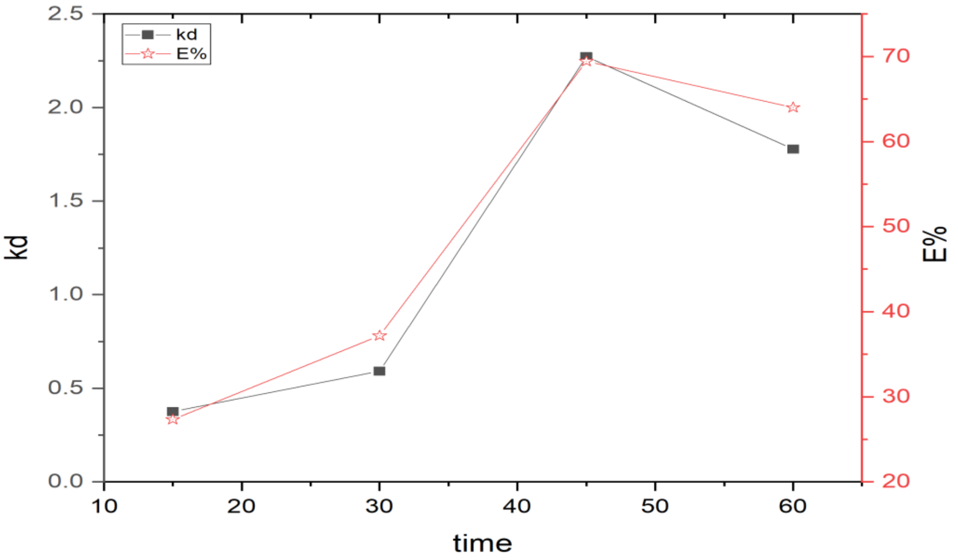

Fig. 5. Relationship between E% and kd vs contact time (min) for adsorption direct orange 39 dye on synthesis $CoFe_2O_4$ nanoparticles

at a constant dye concentration. This can be attributed to the fact that a higher catalyst dosage results in a larger active surface area, thereby enhancing the opportunity for dye removal from the solution [39]. However, it should be noted that the removal capacity (qe) decreased when the mass of $CoFe_2O_4$ was more than 0.4 g due to an increase in turbidity caused by the higher mass of the catalyst and the limitation of active sites on the catalyst surface [40].

Effect of Temperature on direct orange39 dye Removal process

The information provided in Fig. 8 unveils the

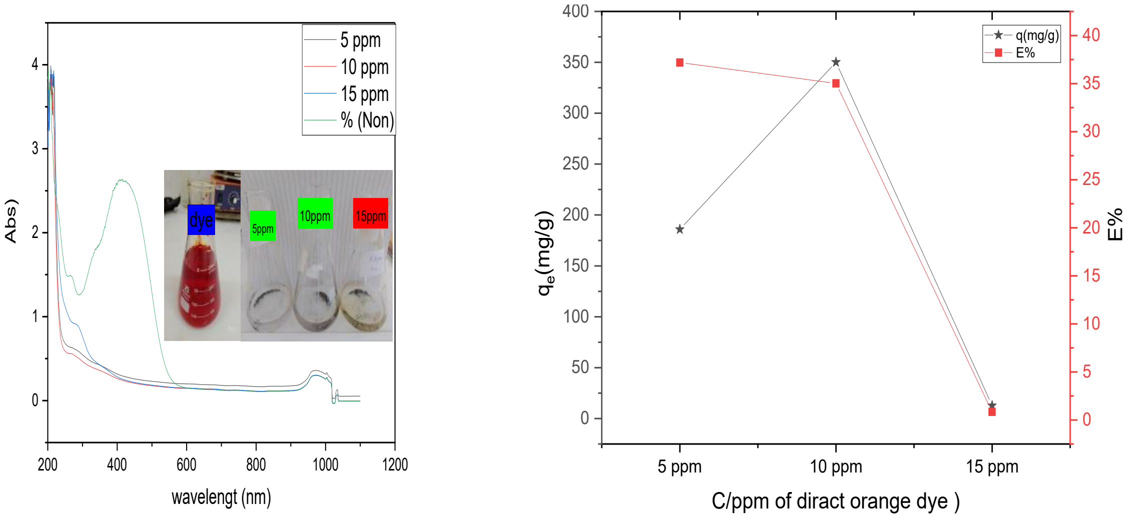

Fig. 6.(a) The relationship between (Abs) and wavelength of the different concentrations (b) the relationship between(E%) and (qe) with different concentrations of dye.

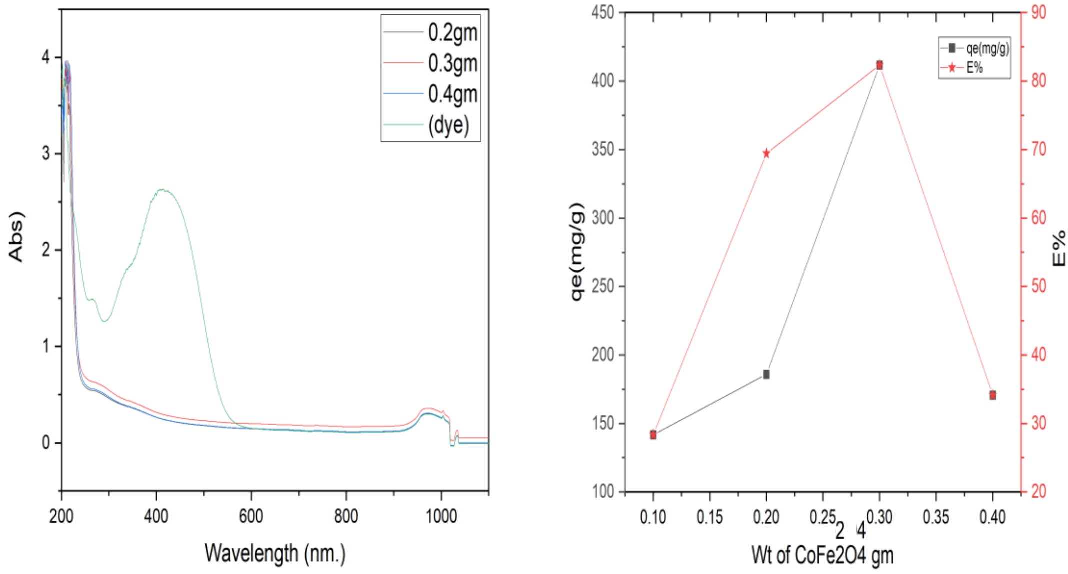

Fig. 7. The relationship between (Abs) and wavelength and for the various doses (b) The relationship between (E%) and (qe) with dose of $CoFe_2O_4$ NPs.

profound effect of temperature on adsorption. A wonderful tremendous correlation is observed between temperature and adsorption performance, with the highest efficiency of 97.82 % executed at 10°C. Concomitantly, the adsorption capacity exhibited a trend, achieving a maximum of 10°C. This temperature dependence may be attributed to the improved mobility and reactivity of the dye molecules and the nanoparticle surface at better temperatures, facilitating extra efficient adsorption and subsequent adsorption. The adsorption efficiency decreased with elevating the temperature, reaching 82.34% at 25°C, which indicated the reaction was exothermic. [41,42].

Thermodynamic Parameters

The adsorption process is significantly affected by changes in temperature, which can either enhance or diminish its effects by specific types of adsorptions. By utilizing the Van't Hoff formula, as shown in Fig. 9, it becomes possible to calculate crucial thermodynamic parameters such as the increase in entropy (ΔH^o) and variation in the thermodynamics of adsorption (ΔS^o) [43]:

$$\ln k_d = \frac{-\Delta H^\circ}{RT} + \frac{\Delta s^\circ}{R} \qquad (4)$$

Here, R stands for the universal gas constant (J/mol. K) and T is the absolute temperature in Kelvin.

Using the Nernst equation (equation 5), the standard Gibbs free energy (ΔG°) was determined, and the relation between ΔG° and temperature is plotted in Fig. 10.

$$\Delta G^o = -RT\ln k_d \qquad (5)$$

However, equation) 6(was used to get the activation energy (Ea) [44].

$$E_a = \Delta H^o + RT \qquad (6)$$

It can be concluded from Figs. 9 and 10 and Table 3, that the processes are thermal and

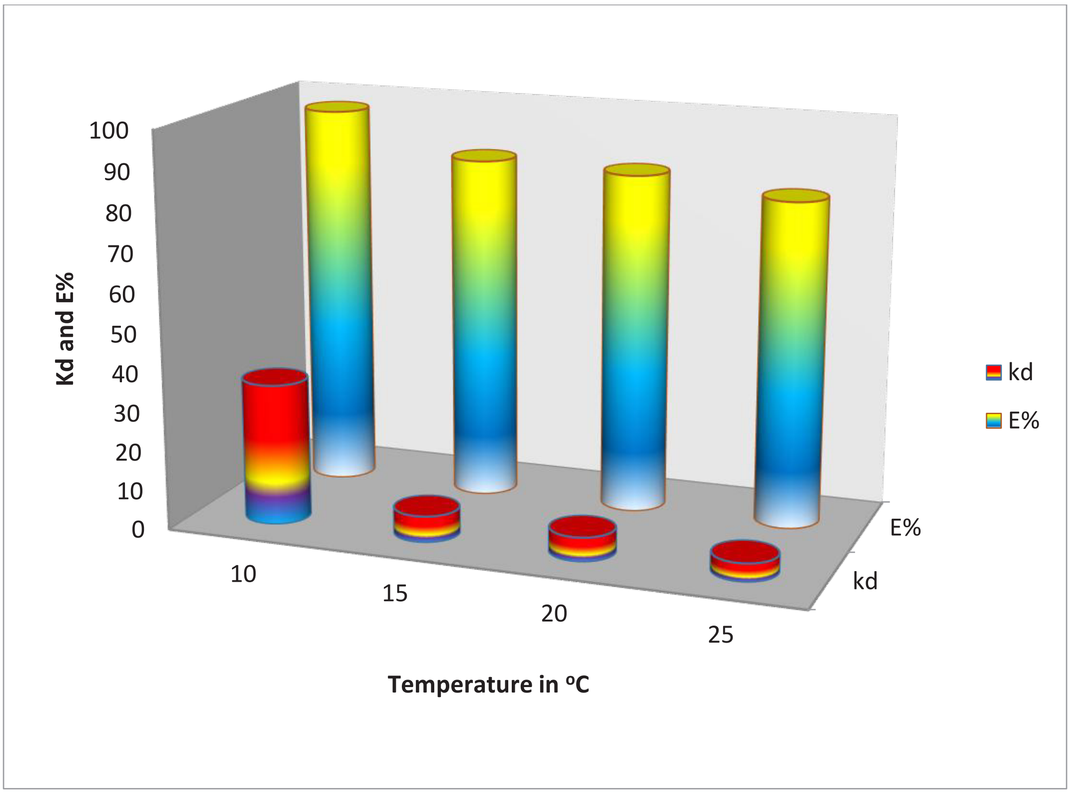

Fig. 9. Relationship between lnk_d and 1000/T during direct orange 39 dye removing via $CoFe_2O_4$ NPs.

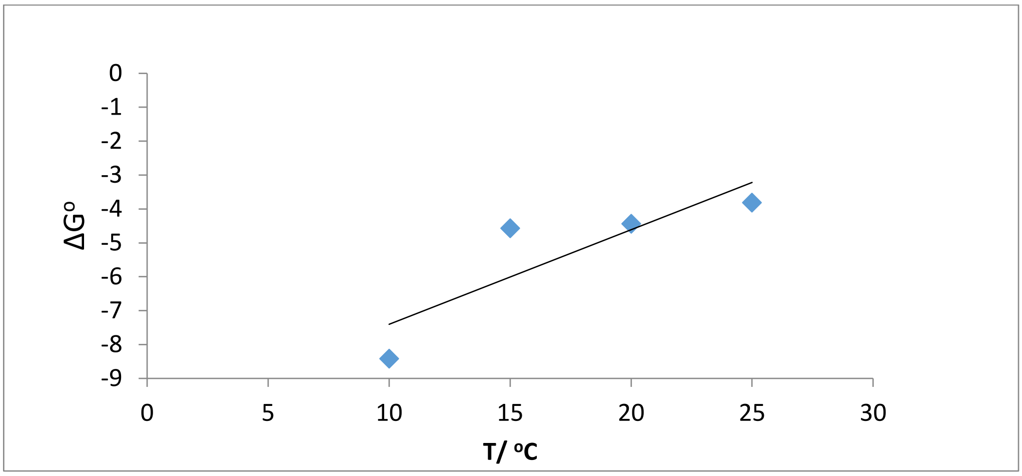

Fig. 10. The variability of Gibb's free energy changes (ΔG) for direct orange 39 dye removing from the $CoFe_2O_4$ surface at various temperatures.

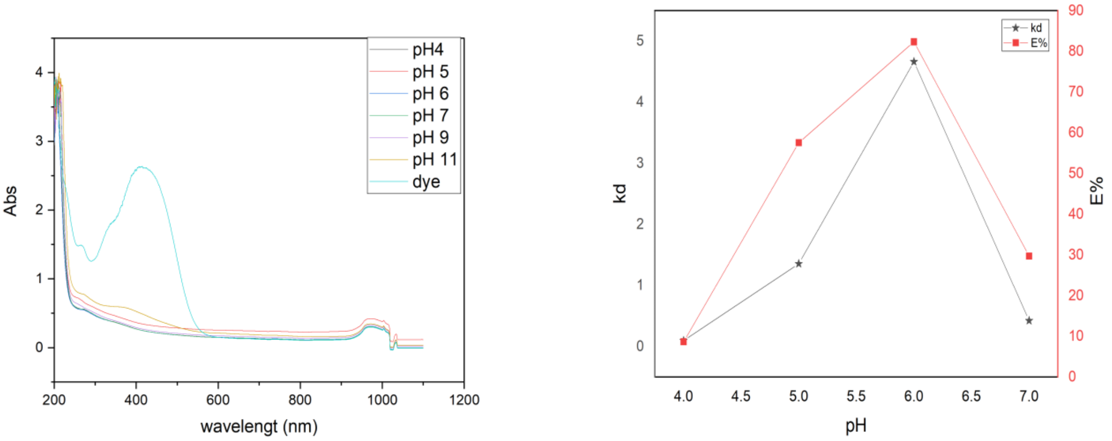

Fig. 11. (a) The relationship between (Abs) and (wavelength)for dye solution at different pH (b) The relationship between (E %) and (kd) with different pH of dye solution.

Table 3. Kinetic and thermodynamic variables for adsorption of direct orange 39 dyes on $CoFe_2O_4$ surfaces.

ΔHo kJ mol^{-1}	ΔSo kJ mol^{-1}	ΔGo kJ mol^{-1}	E_a kJ mol^{-1}
-87.646	**-0.283**	-8.419	-85.293
		-4.572	-85.251
		-4.437	-85.210
		-3.814	-85.168

happened as a physical adsorption depended on ΔHº value. Also the negative value of entropy of the standard, ΔS°, which is -0.28343 kJ mol^{-1}, refers to a decrease in the randomness. The negative sign of ΔGº reveals that the adsorption process is spontaneous. These data showed that the adsorption process proceeded through an associative-type process and did not result in any alteration to the internal framework of the catalyst ($CoFe_2O_4$) [45]. The negative value of activation energy indicates the uptake of dye from solution is a fast reaction, moreover that may be interpreted to find multi-step binding on $CoFe_2O_4$ surface because it contains two different ions with different oxidation states and they demonstrate two different hybridization (tetrahedral and octahedral) in FT-IR analysis.

Effect of pH of direct orange 39 dye on the Adsorption Process

Modification of acidity is a key factor in effectively removing dyes from water-based solutions. According to the data presented in Fig. 11, the highest level of removal (82.3429%) was achieved at pH 6. However, if the pH exceeds this value, the percentage removal starts to decline. This decrease can be attributed to the presence of a negative charge on the surface of $CoFe_2O_4$ when exposed to a strongly alkaline environment, which leads to the formation of the $[Co(OH)_4]^{2-}$ complex [23,24]. The presence of a high concentration of hydrogen ions, that is, an acidic environment, causes the dispersion of positive charges onto the surface of the $CoFe_2O_4$, resulting in the generation of $CoOH^+$ or Co^{2+} ions [6].This results in competition between dye molecules and hydrogen ions for the active sites of the $CoFe_2O_4$.

Reusability of $CoFe_2O_4$ nanoparticles

The statistics provided in Fig. 12 on the reusability of the synthesized $CoFe_2O_4$ NPs .three times reused, the efficiency depressless then 32.776%, and with continuous use it for five runs that will decline less than 20.882% a gradual decline in performance become found with subsequent reuse cycles. This phenomenon can be ascribed to the capacity deactivation by saturated or blocking the active sites of the surface by dye molecules, or fouling of the nanoparticle surface, which may restrict the adsorption and adsorption strategies [45]. Nevertheless, the nanoparticles proven ability to perform well during the first three rounds pastime more than one cycle, underscoring their potential for sustainable and fee-effective applications. The results indicate a decline in adsorption efficiency with continuous reuse cycle when used five times. it maintained its warranty until the third time because the dye molecules gradually accumulate and prevent interaction with the surface [46]. However, the

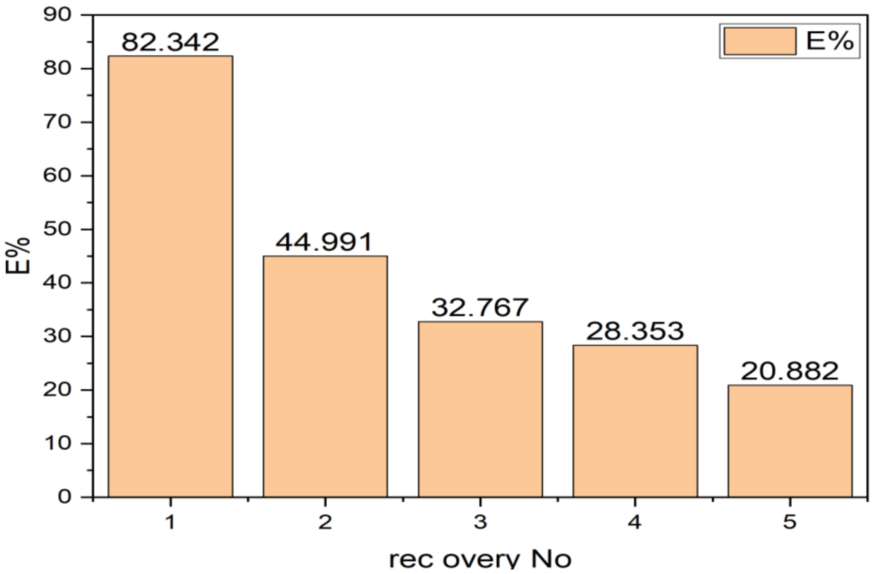

Fig. 12. Reusability of $CoFe_2O_4$NPs surface for direct orange 39 dye adsorption.

fourth time it started to decrease with repeated use. However, the nanoparticles still exhibited significant adsorption activity after multiple cycles. The results observed good reusability, which is the acceptable loss in the sorption ability after five circulations.

CONCLUSION

This study successfully synthesized and characterized $CoFe_2O_4$ nanoparticles using a facile preparation method. The nanoparticles so produced were used to study the removal of direct orange 39 dye from aqueous solution. $CoFe_2O_4$ nanoparticles were synthesized using ferric nitrate and cobalt nitrate in the presence of a positive surfactant, cetramide. The synthesized nanoparticles were characterized via several analytical techniques: FTIR analysis confirmed the spinel structure of $CoFe_2O_4$ and the presence of metal-oxygen bands; XRD analysis verified the phase purity and crystalline nature of the $CoFe_2O_4$ nanoparticles, with a calculated crystallite size of approximately 30.9 nm. SEM analysis revealed a compressed arrangement of homogeneous, roughly textured nanoparticles with a size of around 41.35 nm, is consistent with their polycrystalline nature. EDX analysis confirmed the elemental composition of the nanoparticles, indicating high purity with no significant impurities. The efficiency of $CoFe_2O_4$ nanoparticles in removing direct orange 39 dye was evaluated under varying conditions of dye concentration, nanoparticle dose, pH, and temperature. The effect of increasing dye concentration was that the elimination efficiency decreased from 37.18% to 0.85% The starting dye concentration was increased from 5 ppm to 15 ppm, indicating saturation of active sites on the catalyst surface. The effect of nanoparticle dose was that increasing the dose of $CoFe_2O_4$ nanoparticles improved the dye removal efficiency up to 82.34% at a dose of 0.3 g/100 mL, beyond which the efficiency decreased due to increased turbidity. The effect of pH was that the highest removal efficiency was observed at pH 6, with an overall decrease in efficiency at higher pH due to changes in surface charge and competition between dye molecules and hydrogen ions. The effect of temperature was that the adsorption process was found to be exothermic, with negative thermodynamic parameters indicating spontaneous and associative adsorption without altering the internal structure of the catalyst. In conclusion, the $CoFe_2O_4$ nanoparticles synthesized in this study demonstrated the effective elimination of direct orange 39 dyes from aqueous solution. The adsorption efficiency was, as noted above in detail, influenced by factors such as dye concentration, nanoparticle dose, pH, and temperature. The negative thermodynamic values indicated an exothermic and spontaneous adsorption process, confirming the potential of $CoFe_2O_4$ nanoparticles to act as an efficient adsorbent for dye removal in water treatment applications. The current research validates the potential of $CoFe_2O_4$ nanoparticles as effectual, reusable adsorbents for water treatment, advancing cost-effective resolutions for dye elimination. It contributes to nanotechnology by highlighting the application of magnetic spinal ferrites in sustainable water purification.

CONFLICT OF INTEREST

The authors declare that there is no conflict of interests regarding the publication of this manuscript.

REFERENCES

1. Hassan SA, Almaliki MN, Hussein ZA, Albehadili HM, Rabeea Banoon S, Abboodi A, Al-Saady M. Development of nanotechnology by artificial intelligence: a comprehensive review. Journal of Nanostructures. 2023 ;13(4):915-932.
2. Ali ZH, Al-Saady MA, Aldujaili NH, Rabeea Banoon S, Abboodi A. Evaluation of the antibacterial inhibitory activity of chitosan nanoparticles biosynthesized by streptococcus thermophilus. Journal of Nanostructures. 2022;12(3):675-685.
3. Abed AQ, Hindawi AMA, Alesary HF. Synthesis and characterization of zinc sulfide nanomaterials for removal methylene blue dye from aqueous solution. AIP Conference Proceedings: AIP Publishing; 2023. p. 020001.
4. Al-Fiydh MN, Najm HF, Karam FF, Baqir SJ. Thermodynamics, kinetic study and equilibrium isotherm analysis of cationic dye adsorption by ternary composite. Results in Chemistry. 2024;10:101680.
5. Ali LIA, Ismail HK, Alesary HF, Aboul-Enein HY. A nanocomposite based on polyaniline, nickel and manganese oxides for dye removal from aqueous solutions. Int J Environ Sci Technol (Tehran). 2020;18(7):2031-2050.
6. Alijani HQ, Iravani S, Pourseyedi S, Torkzadeh-Mahani M, Barani M, Khatami M. Biosynthesis of spinel nickel ferrite nanowhiskers and their biomedical applications. Sci Rep. 2021;11(1):17431-17431.
7. Aljeboree AM, Abdulrazzak FH, Alkaim AF, Hussein FH. Advanced Oxidation Process as a type of photo catalytic removal of Maxilon blue dye (GRL) using. Journal of Physics: Conference Series. 2020;1664(1):012096.
8. Batana FZ, Babaghayou MI, Zoukel A, Karef S. Removal of two cationic dyes by adsorption on F400 commercial activated carbon. Studies In Engineering and Exact Sciences. 2024;5(2):e6185.
9. Chen W, Lu W, Yao Y, Xu M. Highly Efficient Decomposition of Organic Dyes by Aqueous-Fiber Phase Transfer and in Situ Catalytic Oxidation Using Fiber-Supported Cobalt Phthalocyanine. Environmental Science and Technology. 2007;41(17):6240-6245.
10. Ding Y, Yang Y, Shao H. High capacity $ZnFe_2O_4$ anode material for

lithium ion batteries. Electrochimica Acta. 2011;56(25):9433-9438.

11. Ghasemian E, Palizban Z. Comparisons of azo dye adsorptions onto activated carbon and silicon carbide nanoparticles loaded on activated carbon. Int J Environ Sci Technol (Tehran). 2015;13(2):501-512.
12. Gong R, Li M, Yang C, Sun Y, Chen J. Removal of cationic dyes from aqueous solution by adsorption on peanut hull. J Hazard Mater. 2005;121(1-3):247-250.
13. Gul IH, Maqsood A. Structural, magnetic and electrical properties of cobalt ferrites prepared by the sol–gel route. J Alloys Compd. 2008;465(1-2):227-231.
14. Gutiérrez MC, Pepió M, Crespi M. Electrochemical oxidation of reactive dyes: method validation and application. Coloration Technology. 2002;118(1):1-5.
15. Hussain ZA, Fakhri FH, Alesary HF, Ahmed LM. ZnO Based Material as Photocatalyst for Treating the Textile Anthraquinone Derivative Dye (Dispersive Blue 26 Dye): Removal and Photocatalytic Treatment. Journal of Physics: Conference Series. 2020;1664(1):012064.
16. Jaafar MT, Ahmed LM. Reduced the toxicity of acid black (nigrosine) dye by removal and photocatalytic activity of TiO$_2$ and studying the effect of pH, temperatue, and the oxidant agents. AIP Conference Proceedings: AIP Publishing; 2020. p. 030034.
17. Abd Zaid AA, Ahmed LM, Mohammad RK. Synthesis of inverse spinel nickel ferrite like-broccoli nanoparticle and thermodynamic study of photo-decolorization of alkali blue 4B dye. Journal of Nanostructures. 2022;12(3):697-710.
18. Abd Zaid AA, Ahmed LM, Mohammad RK. Solvothermal-assisted cushy precipitation method of like-cauliflower zinc ferrite (ZnFe$_2$O4) nanoparticles using hexamethylenetetramine (hexamine) as a non-ionic surfactant. Journal of Nanostructures. 2023;13(1):193-203.
19. Hameed M.A. and Ahmed L.M., 2024. SDS-Assisted Hydrothermal Growth and Photocatalytic Activity of Like-Caviar MoFe 2 O 4 Nanoparticle Decorated with Al$_2$O$_3$. Indonesian Journal of Chemistry, 24(3): 776-790.
20. Hameed, M.A. and Ahmed, L.M., Controllable Cetrimide–Assisted Hydrothermal Synthesis of MoFe$_2$O$_4$ and Coupling with Al$_2$O$_3$ as an Effective Photocatalyst for Decolorization of Indigo Carmine Dye. Indonesian Journal of Chemistry, 24(1):170-184.
21. Tarq N., Sadoon H. and Alshammari A., (2024). Characterization of cobalt ferrite nanoparticle and evaluation its toxic effect in experimental mice. Acta Veterinaria Brasilica, 18(2): 103-110.
22. Kalam A., Al-Sehemi A.G., Assiri M., Du, G., Ahmad, T., Ahmad, I. and Pannipara, M., (2018). Modified solvothermal synthesis of cobalt ferrite (CoFe$_2$O$_4$) magnetic nanoparticles photocatalysts for degradation of methylene blue with H2O2/visible light. Results in physics, 8, pp.1046-1053.
23. Maaz K, Mumtaz A, Hasanain SK, Ceylan A. Synthesis and magnetic properties of cobalt ferrite (CoFe$_2$O$_4$) nanoparticles prepared by wet chemical route. J Magn Magn Mater. 2007;308(2):289-295.
24. Saeed SI, Attol DH, Eesa MT, Ahmed LM. Zinc oxide-mediated removal and photocatalytic treatment of direct orange 39 dye as a textile dye. InAIP Conference Proceedings 2023(Vol. 2414, No. 1). AIP Publishing.
25. Oda AM, Khudheyer FY, Obaid EK. Photocatalytic Decolorization of Crystal Violate Dye Solution by ZnO/MWCNT Nanocomposite. Iraqi Journal of Science. 2023:3748-3762.
26. Mohammad HM, Saeed SI, Ahmed LM. Broccolilike iron oxide nanoparticles synthesis in presence of surfactants and using them in the removal of water-colored contamination. Journal of Nanostructures. 2022;12(4):1034-1048.
27. Anandan K, Rajesh K, Rajendran V. Size, morphology and optical properties of zirconia (ZrO$_2$) nanostructures synthesized via the facile ionic surfactant-assisted solvothermal method. Journal of Materials Science: Materials in Electronics. 2017;28(18):13420-13425.
28. Mustafa G, Islam MU, Zhang W, Jamil Y, Anwar AW, Hussain M, et al. Investigation of structural and magnetic properties of Ce^{3+}-substituted nanosized Co–Cr ferrites for a variety of applications. J Alloys Compd. 2015;618:428-436.
29. Mathew DS, Juang RS. An overview of the structure and magnetism of spinel ferrite nanoparticles and their synthesis in microemulsions. Chemical engineering journal. 2007;129(1-3):51-65.
30. Goodarz Naseri M, Saion EB, Kamali A. An overview on nanocrystalline ZnFe$_2$O$_4$, MnFe$_2$O$_4$, and CoFe$_2$O$_4$ synthesized by a thermal treatment method. International Scholarly Research Notices. 2012;2012(1):604241.
31. Gu Z, Xiang XU, Fan G, Li F. Facile synthesis and characterization of cobalt ferrite nanocrystals via a simple reduction-oxidation route. The Journal of Physical Chemistry C. 2008 , 27;112(47):18459-66.
32. Goodarz Naseri M, Saion EB, Abbastabar Ahangar H, Shaari AH, Hashim M. Simple Synthesis and Characterization of Cobalt Ferrite Nanoparticles by a Thermal Treatment Method. Journal of Nanomaterials. 2010;2010(1).
33. Nasir AM, Goh PS, Abdullah MS, Ng BC, Ismail AF. Adsorptive nanocomposite membranes for heavy metal remediation: Recent progresses and challenges. Chemosphere. 2019;232:96-112.
34. Rajput AB, Hazra S, Ghosh NN. Synthesis and characterisation of pure single-phase CoFe$_2$O$_4$ nanopowder via a simple aqueous solution-based EDTA-precursor route. J Exp Nanosci. 2012;8(4):629-639.
35. Obaid, A. and Ahmed, L., One-step hydrothermal synthesis of α-MoO$_3$ nano-belts with ultrasonic assist for incorporating TiO$_2$ as a nanocomposite. Egyptian Journal of Chemistry. 64(10), 2021: 5725-5734.
36. Kadhim, H., Ahmed, L. and AL-Hachamii, M., Facile Synthesis of Spinel CoCr2O4 and Its Nanocomposite with ZrO$_2$: Employing in Photo--catalytic Decolorization of Fe (II)-(luminol-Tyrosine) Complex. Egyptian Journal of Chemistry. 65(1), 2022:481-488.
37. Saati M, Hamidi S, Jarolmasjed N, Rezvani Z, Davari S. Preparation of Novel Ceo$_2$/Nio/NiAl$_2$O$_4$ Nanocomposite for Fast and Efficient Removal of Direct Red 23: Mechanism, Kinetic, Thermodynamic and Equilibrium Studies. SSRN Electronic Journal. 2022.
38. Sadeghi M, Irandoust M, Khorshidi F, Feyzi M, Jafari F, Shojaeimehr T, et al. Removal of Arsenic (III) from natural contaminated water using magnetic nanocomposite: kinetics and isotherm studies. Journal of the Iranian Chemical Society. 2016;13(7):1175-1188.
39. Shokry F, El-Gedawy M, Nosier SA, Abdel-Aziz MH. Optimizing photocatalytic degradation of methyl violet dye in a recirculating slurry-type reactor. Results in Chemistry. 2025;13:101980.
40. Safi R, Ghasemi A, Shoja-Razavi R, Tavousi M. The role of pH on the particle size and magnetic consequence of cobalt ferrite. J Magn Magn Mater. 2015;396:288-294.
41. Saha P, Chowdhury S. Insight Into Adsorption Thermodynamics. Thermodynamics: InTech; 2011.
42. Sharma RK, Suwalka O, Lakshmi N, Venugopalan K, Banerjee A, Joy PA. Synthesis of chromium substituted nano particles of cobalt zinc ferrites by coprecipitation. Mater Lett. 2005;59(27):3402-3405.
43. Potgieter JH, Pardesi C, Pearson S. A kinetic and thermodynamic investigation into the removal of methyl orange from wastewater utilizing fly ash in different process configurations. Environmental Geochemistry and Health. 2021;43:2539-2550.
44. Taty-Costodes VC, Fauduet H, Porte C, Delacroix A. Removal of Cd(II) and Pb(II) ions, from aqueous solutions, by adsorption onto sawdust of Pinus sylvestris. J Hazard Mater. 2003;105(1-3):121-142.
45. Trivedi UN, Jani KH, Modi KB, Joshi HH. J Mater Sci Lett. 2000;19(14):1271-1273.
46. Zhang Z-h, Zhang J-l, Liu J-m, Xiong Z-h, Chen X. Selective and Competitive Adsorption of Azo Dyes on the Metal–Organic Framework ZIF-67. Water, Air, and Soil Pollution. 2016;227(12).